Inclined nanoimprinting lithography-based 3D nanofabrication



2011 J. Micromech. Microeng. 21 065036

(http://iopscience.iop.org/0960-1317/21/6/065036)

IOP PUBLISHING JOURNAL OF MICROMECHANICS AND MICROENGINEERING

J. Micromech. Microeng. **21** (2011) 065036 (11pp) doi:10.1088/0960-1317/21/6/065036

# Inclined nanoimprinting lithography-based 3D nanofabrication

**Zhan Liu**[1,3], **David G Bucknall**[1] **and Mark G Allen**[2]

[1] School of Materials Science and Engineering, Georgia Institute of Technology, Atlanta, GA 30332, USA

[2] School of Electrical and Computer Engineering, Georgia Institute of Technology, Atlanta, GA 30332, USA

E-mail: zhan.liu@gatech.edu

Received 22 February 2011, in final form 28 March 2011
Published 18 May 2011
Online at stacks.iop.org/JMM/21/065036

**Abstract**

We report a 'top–down' 3D nanofabrication approach combining non-conventional inclined nanoimprint lithography (INIL) with reactive ion etching (RIE), contact molding and 3D metal nanotransfer printing (nTP). This integration of processes enables the production and conformal transfer of 3D polymer nanostructures of varying heights to a variety of other materials including a silicon-based substrate, a silicone stamp and a metal gold (Au) thin film. The process demonstrates the potential of reduced fabrication cost and complexity compared to existing methods. Various 3D nanostructures in technologically useful materials have been fabricated, including symmetric and asymmetric nanolines, nanocircles and nanosquares. Such 3D nanostructures have potential applications such as angle-resolved photonic crystals, plasmonic crystals and biomimicking anisotropic surfaces. This integrated INIL-based strategy shows great promise for 3D nanofabrication in the fields of photonics, plasmonics and surface tribology.

(Some figures in this article are in colour only in the electronic version)

## 1. Introduction

Fabrication of various well-defined 3D nanostructures with controlled feature sizes is a significant technical driver for a number of applications in different fields including photonics, plasmonics, nanotribology and nanoelectromechanical systems (NEMS). For example, 3D nanophotonic crystals exploit periodic 3D nano-sized dielectric structures to dramatically influence light through them [1–3]. However, it is much more challenging to fabricate high-quality 3D nanophotonic crystals and properly integrate them in optical devices compared to 1D/2D nanophotonic crystals. Some 'top–down' nanolithographic techniques have shown their fabrication potentials including electron beam lithography (EBL) [4, 5], laser direct writing [2, 6], nanoimprinting lithography (NIL) and photolithography using phase masks [7]. However, process speed (e.g. for EBL and laser direct writing), increased process complexity (e.g. multiple alignments between layers) as well as potential high cost are practical barriers inhibiting their application to fields such as photonics.

The emerging field of plasmonic crystals is another example of increasing research activity requiring highly defined micro/nanostructures. Plasmonic crystals have metallic nanostructures, where confined electrons are forced to oscillate by an incident light or electromagnetic wave. Such electron oscillation can exhibit strong local-field enhancement at a particular wavelength known as localized surface plasmon resonances (LSPRs). This electron–photon coupled resonance is essential to increase nearly all light–matter interactions including surface-enhanced Raman scattering (SERS) and surface-enhanced fluorescence for applications including bio-diagnostics, imaging and sensing [8–14]. The plasmon resonance frequency is largely determined by the metal nanostructure itself [13]. Therefore, there is a surge of interest in exploring proper nanofabrication approaches that can control the shape, size and spacing of metal structures at micro/nano scales, e.g. in three dimensions.

[3] Author to whom any correspondence should be addressed.

 

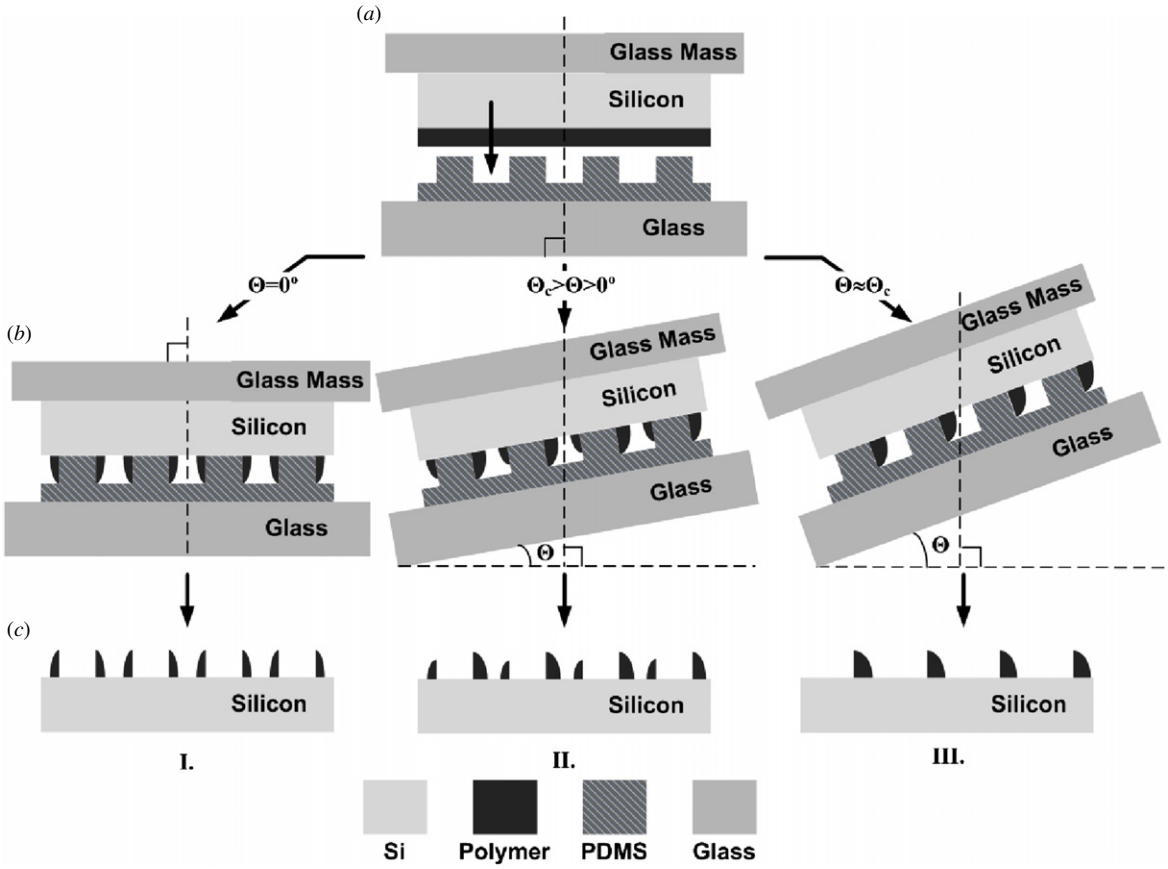


**Figure 1.** Schematic illustration of the INIL fabrication process (I) $\theta = 0^\circ$, (II) $0^\circ < \theta < \theta_c$, (III) $\theta \approx \theta_c$ ($\approx 5^\circ$). (*a*) An intimate contact between the Si substrate spin coated with a polymer thin film and the PDMS stamp; (*b*) inclining the assembly by $\theta^\circ$ and annealing it at a temperature higher than the polymer glass transition temperature for a few hours; (*c*) cooling down the assembly and separating the substrate from the PDMS stamp.

Recently, we demonstrated a non-conventional shear-force-driven nanofabrication approach, inclined nanoimprint lithography (INIL) [15]. It enables the production of various 3D polymer nanostructures of varying heights on a planar substrate in a single imprinting step. In this paper, we describe the use of such 3D polymer nanostructures, which have been conformally transferred to silicon (Si) substrate, PDMS (poly(dimethyl siloxane)) silicone and metal gold (Au) thin film by integrating INIL with reactive ion etching (RIE), micro-contact molding ($\mu$CM) and 3D metal nanotransfer printing (nTP) [16]. Nanolithography polymer resist ZEP520 (Zeon Chemicals L. P.) [17], poly(methyl-$\alpha$-chloroacrylate-*co*-$\alpha$-methylstyrene), was used as the INIL resist due to its more amenable material properties for post-INIL processing by reactive ion dry etching. This INIL-based 3D nanofabrication strategy enables the 'top–down' production of angle-resolved photonic crystals, plasmonic crystals and anisotropic self-cleaning surfaces in a designated way.

## 2. Fabrication

### *2.1. Inclined INIL*

The INIL fabrication process is outlined in figure 1, with full details found elsewhere [15]. In summary, a micro-patterned PDMS stamp (e.g. trenches 1 $\mu$m width, 1 $\mu$m depth and 2 $\mu$m lateral pitch separation; square columns 1 $\mu$m width and 2 $\mu$m lateral pitch separation, and cylindrical pillars 1 $\mu$m diameter, 1 $\mu$m depth and 2 $\mu$m lateral pitch separation) is first treated by $O_2$ plasma and brought into contact with a thin ZEP520 film spun on a silicon substrate. Intimate contact between the PDMS stamp and the ZEP520 film is maintained by loading with a glass plate on the top surface (figure 1(*a*)). The entire assembly is then inclined at a small angle $\theta$ e.g. between $0^\circ$ and $5^\circ$, and annealed for several hours in vacuum at a temperature above the ZEP520 glass transition temperature ($T_g = 105\,^\circ$C), e.g. 170 °C for approximately 12 h, 190 °C for approximately 5 h, 230 °C for 2–3 h [22]. During the annealing, the polymer flows and tends to dewet from the Si substrate, preferentially wetting the PDMS sidewalls. When $\theta = 0^\circ$ (figure 1I), this dewetting–wetting process results in a symmetric polymer flow, and consequently a symmetric polymer cross-sectional profile with nanometer feature sizes of the same height is produced (figure 1I(*b*)). The patterned film is revealed by cooling the assembly to room temperature and removing the PDMS stamp (figure 1I(*c*)). Increasing $\theta$ above $0^\circ$ consequently leads to asymmetric dewetting behavior of the polymer flow (figure 1II), and as a result, 3D nanopatterns with different heights and widths are obtained (figure 1II(*c*)).

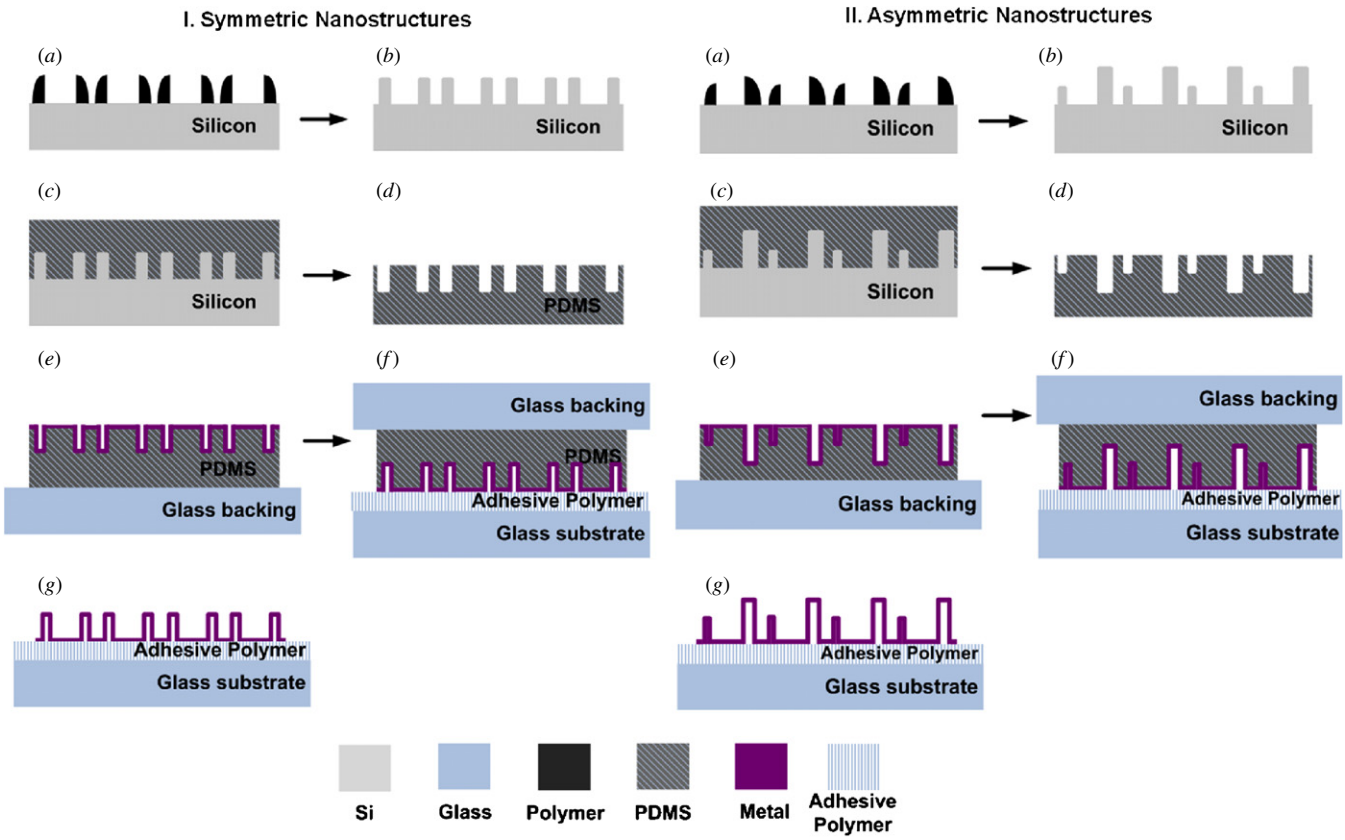


**Figure 2.** Schematic illustration of the INIL-based fabrication process. (*a*) 3D polymer nanostructures produced by INIL; (*b*) reactive ion etching (RIE) for pattern transfer to the Si substrate; (*c*) casting and curing PDMS prepolymer against Si master template; (*d*) de-molding to obtain the PDMS silicon stamp; (*e*) sputtering Au/Ti thin film on the PDMS stamp surface; (*f*) 3D metal nanotransfer printing (nTP) to transfer 3D freestanding Au nanostructures on an adhesive polymer substrate; (*g*) stamp separation.

When $\theta$ is increased close to or beyond a threshold angle $\theta_c$, which is approximately equal to 5°, wetting only occurs on one face of the PDMS (figure 1III(*b*)); consequently, extremely asymmetric 3D nanopatterns can be obtained (figure 1III(*c*)).

### 2.2. *3D nanofabrication based on INIL*

Figure 2 schematically illustrates the INIL-based fabrication process for 3D nanopattern transfer. The process exploits the 3D polymer nanostructures (figure 2(*a*)) produced by INIL, described above. A plasma dry etching ($CHF_3/H_2$) process is applied to transfer the polymer nanopattern to the underlying Si substrate, followed by removal of the polymer residue using either plasma dry etching ($CHF_3/O_2$) or solution cleaning (98% $H_2SO_4$ and 30% $H_2O_2$ in volume ratio of 3:1 at 120 °C for 10 min) (figure 2(*b*)). The resulting Si nanostructure is used as a master template for subsequent PDMS contact molding to transfer the opposite Si 3D nanostructures to a PDMS silicone stamp. In this process, PDMS prepolymer (Sylgard 184, Dow Corning) is cast onto the Si template surface, followed by curing at 60 °C for 24 h (figure 2(*c*)). The PDMS stamp with recessed 3D nanostructures is revealed by de-molding from the Si template (figure 2(*d*)). To achieve this, an anti-adhesion agent (3,3,3-trifluoropropyl dimethylchlorosilane) was used to treat the Si template surface prior to applying the PDMS prepolymer in order to prevent adhesion between the Si master template and the cured PDMS, hence improving mold separation. A typical operation for such a surface treatment is to soak the Si template in a liquid anti-adhesion agent for 2–3 min followed by drying the template by $N_2$ gas. The resulting nanopatterned PDMS stamp is then mounted onto a glass substrate and the surface is coated with a uniform thin metal film by sputtering (figure 2(*e*)), e.g. 40 nm gold (Au)/5 nm titanium (Ti) where the Ti functions as an adhesion layer in the subsequent 3D metal nTP process. In the nTP process (figure 2(*f*)) the 3D Au thin film can be thought of as a nanostructured metal sheet. It is able to be transferred to an adhesive polymer substrate (e.g. Kapton tape backed by a glass substrate or photocurable polyurethane (PU) spin coated onto a glass substrate) due to the higher surface energy of the adhesive polymer. Typically, immediately after metal coating the PDMS stamp it is brought into contact with the polymer substrate and a slight pressure is applied. Once contact has been established, the metal layer on the stamp becomes strongly adhered and is transferred to the high surface energy polymer substrate. After stamp separation, freestanding Au nanostructures of varying heights

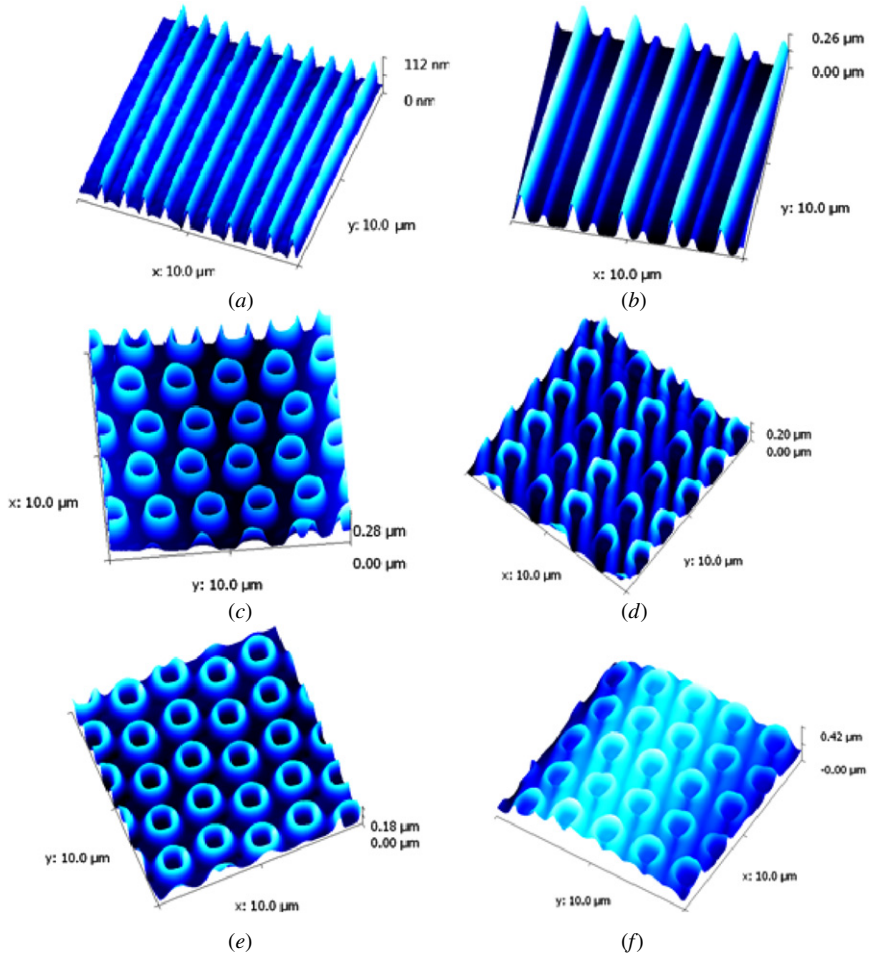


**Figure 3.** AFM images (3D views) of resulting 3D polymer nanostructures produced by INIL. (*a*) Symmetric nanolines; (*b*) asymmetric nanolines; (*c*) symmetric nanocircles; (*d*) asymmetric nanocircles; (*e*) symmetric nanosquares; (*f*) asymmetric nanosquares.

that replicate 3D nanostructures of the Si master template are obtained (figure 2(*g*)).

## 3. Results and discussion

### *3.1. 3D polymer nanostructures*

Figure 3 shows AFM images of resulting polymer 3D nanopatterns of varying heights produced by INIL at different inclination angles. The patterns produced include symmetric and asymmetric nanolines, nanocircles and nanosquares. The height of resulting symmetric nanolines (figure 3(*a*)) produced from a ZEP520 film (30 nm thick) is 100 nm, and the full width half maximum (FWHM) of the lines is 300 nm. The inner diameter of resulting symmetric nanocircles produced from a ZEP520 film (50 nm thick) is 1 $\mu$m, the circle height is approximately 200 nm (figure 3(*c*)) and the FWHM of the circles is 250 nm. The inner side length of resulting symmetric nanosquares produced from a ZEP520 film (70 nm thick) is 1 $\mu$m, the square height is 125 nm and the FWHM of the squares is 400 nm (figure 3(*e*)). Comparison of the volume of the polymer film patterns before and after INIL indicates that the entire polymer mass is properly conserved without any loss in the INIL process. For asymmetric nanolines (figure 3(*b*)), the height and width are varied according to the inclination angle $\theta$, similarly for asymmetric nanocircles (figure 3(*d*)) and nanosquares (figure 3(*f*)), but the total volume of the polymer is still conserved. The actual feature height variation of the resulting asymmetric nanopatterns can be adjusted by tuning the process parameters including the degree of the inclination angle and the initial film thickness. The inclination angle is an essential factor influencing the resulting structure and feature height difference [22]. In this work, the resultant asymmetric nanopattern height difference (e.g. nanolines) ranged from 30 to 200 nm by adjusting the degree of the inclination angle and the initial film thickness for a PDMS mold with a pattern design consisting of trenches 1 $\mu$m in width, 1 $\mu$m in depth and 2 $\mu$m in a lateral pitch separation. In fact, it is also observed that the FWHM of the resulting nanopatterns and the corresponding ratio of height to FWHM are also affected and varied by the inclination angle. Although further study would be needed to understand this behavior quantitatively, we believe it is possible to manipulate the ratio of the height to FWHM of the resultant nanopatterns produced in INIL by carefully manipulating the process factors according to the INIL mechanism.

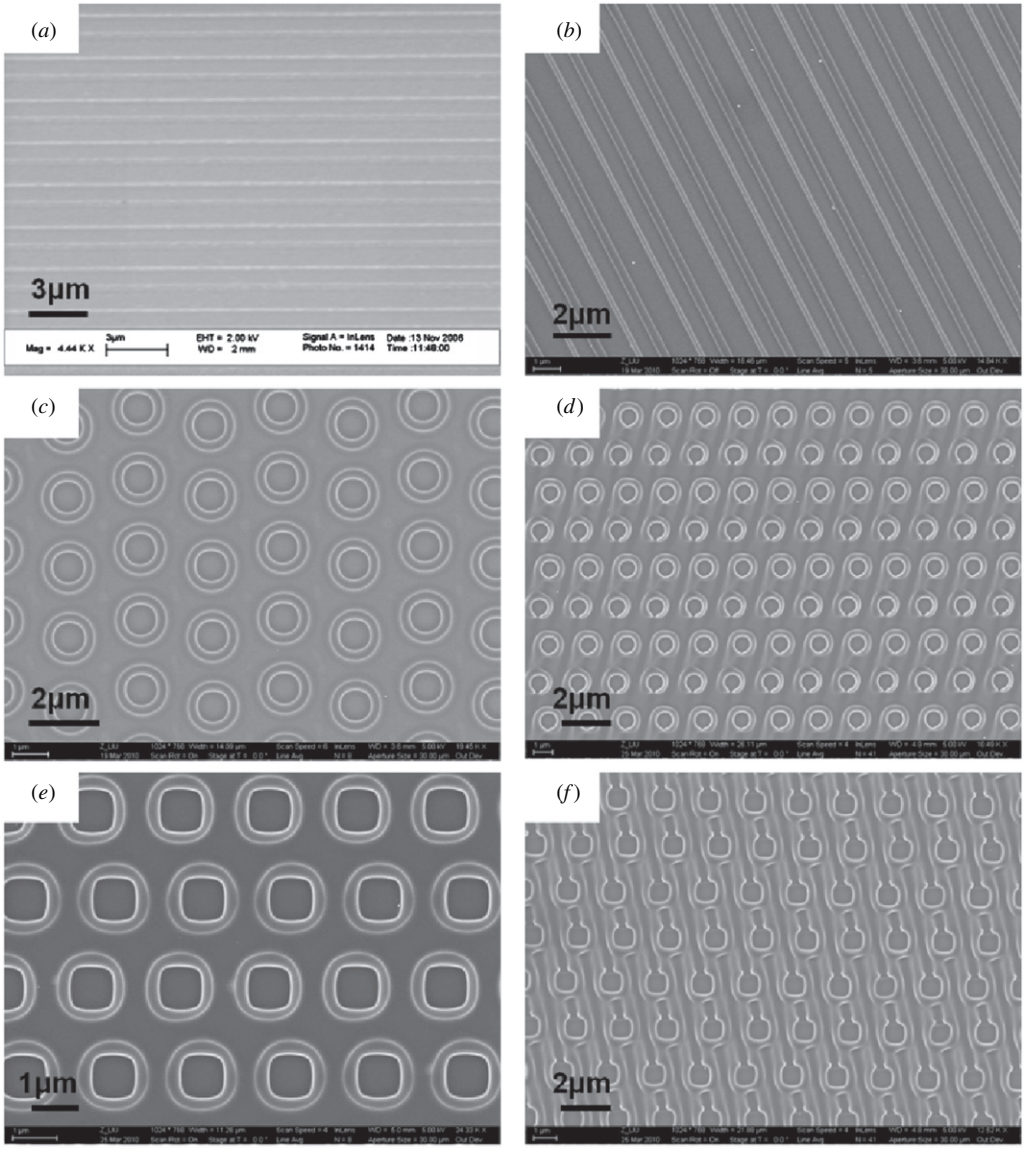


**Figure 4.** SEM images of resulting 3D Si nanostructures. (*a*) Symmetric nanolines; (*b*) asymmetric nanolines; (*c*) symmetric nanocircles; (*d*) asymmetric nanocircles; (*e*) symmetric nanosquares; (*f*) asymmetric nanosquares.

In addition, it can be observed that the corners of the resulting nanosquares are slightly rounded. This is primarily attributed to the PDMS mold, in particular the slight deformation of the mold corners induced by the relaxation of the elastomeric mold material (PDMS, Sylgard 184, Dow Corning). Relaxation occurs after separating the molded PDMS stamp from the Si master in the PDMS mold preparation. Material relaxation is caused by the surface tension, which can deform the molded sharp corners into a smooth equilibrium rounded shape with a radius of curvature ($R_c$) on the order of $\gamma_s$ (surface energy)/E (modulus), and thus $\gamma_s$/E represents a lower limit for $R_c$ of the corners. For a PDMS elastomer $R_c$ is on the order of 50 nm [18]. One possible solution to address the edge rounding issue is the use of a mold material that has a larger modulus (E) such as PDMS composite material [19]. A larger modulus (E) would lead to smaller $R_c$, and thus conformal sharp corners may be retained by the stamp.

While this work mainly focuses on micron or sub-micron nanopattern separation distance, it is theoretically feasible to fabricate 3D nanopatterns with sub-100 nm separation distances by using a sub-100 nm patterned PDMS stamp [19] ($d \leqslant 100$ nm) and also reducing the initial polymer film thickness to 5–10 nm. Smaller film thicknesses would allow polymer dewetting at smaller length scales. Meanwhile, strategies to ensure intimate contact between the stamp and the substrate without deforming the fine features of the PDMS stamp and reduce the adhesion issue at the stamp–substrate separation step also need to be addressed.

Moreover, although uniformity was not quantitatively assessed, visual inspection by SEM indicated no significant uniformity variation over the entire pattern dimension (100 $\mu$m $\times$ 1 mm to 500 $\mu$m $\times$ 3 mm for nanolines, and

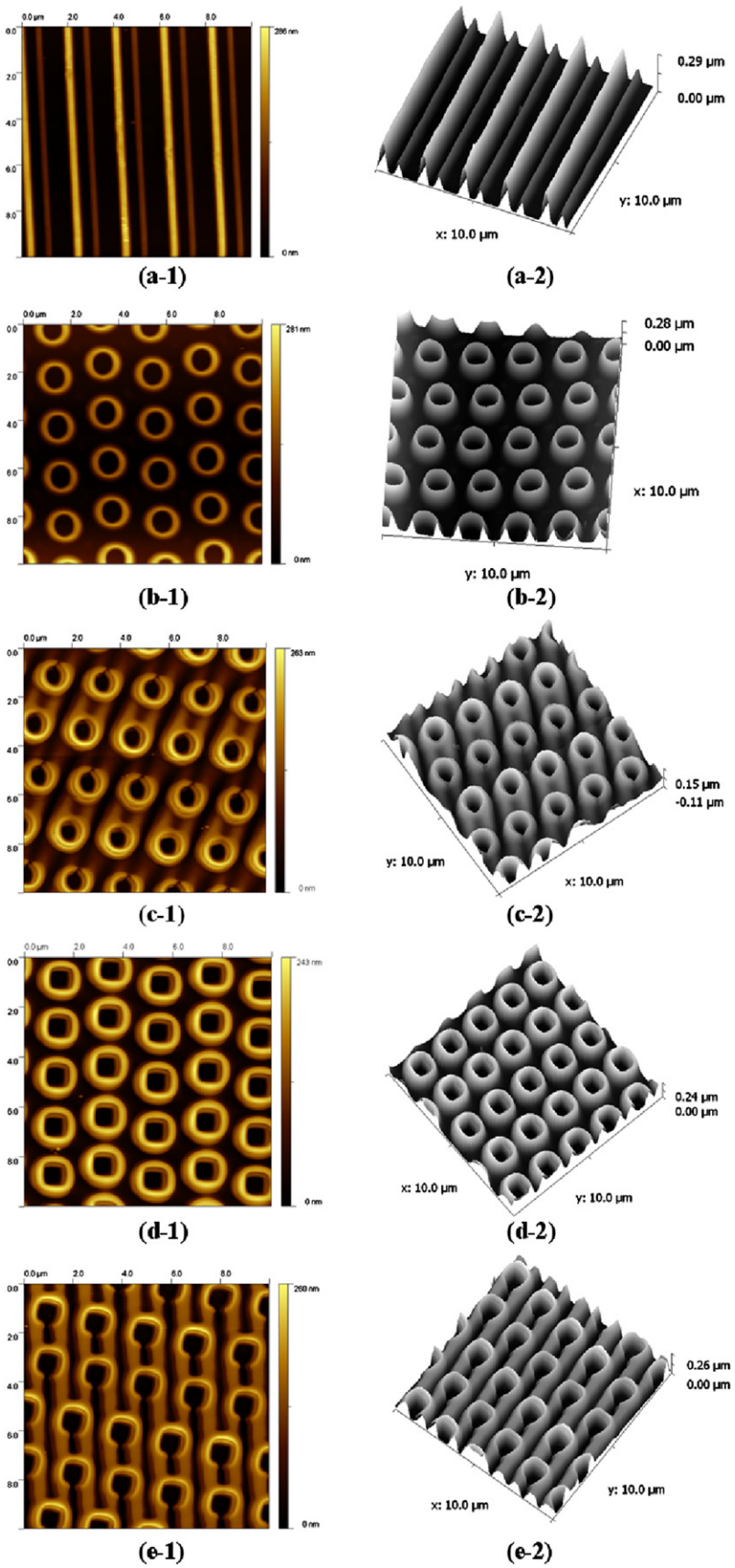


**Figure 5.** AFM images of resulting 3D Si nanostructures in top (left) and 3D (right) views. (*a*-1, *a*-2) Asymmetric nanolines; ((*b*-1, *b*-2) and (*c*-1, *c*-2)) symmetric and asymmetric nanocircles; ((*d*-1, *d*-2) and (*e*-1, *e*-2)) symmetric and asymmetric nanosquares.

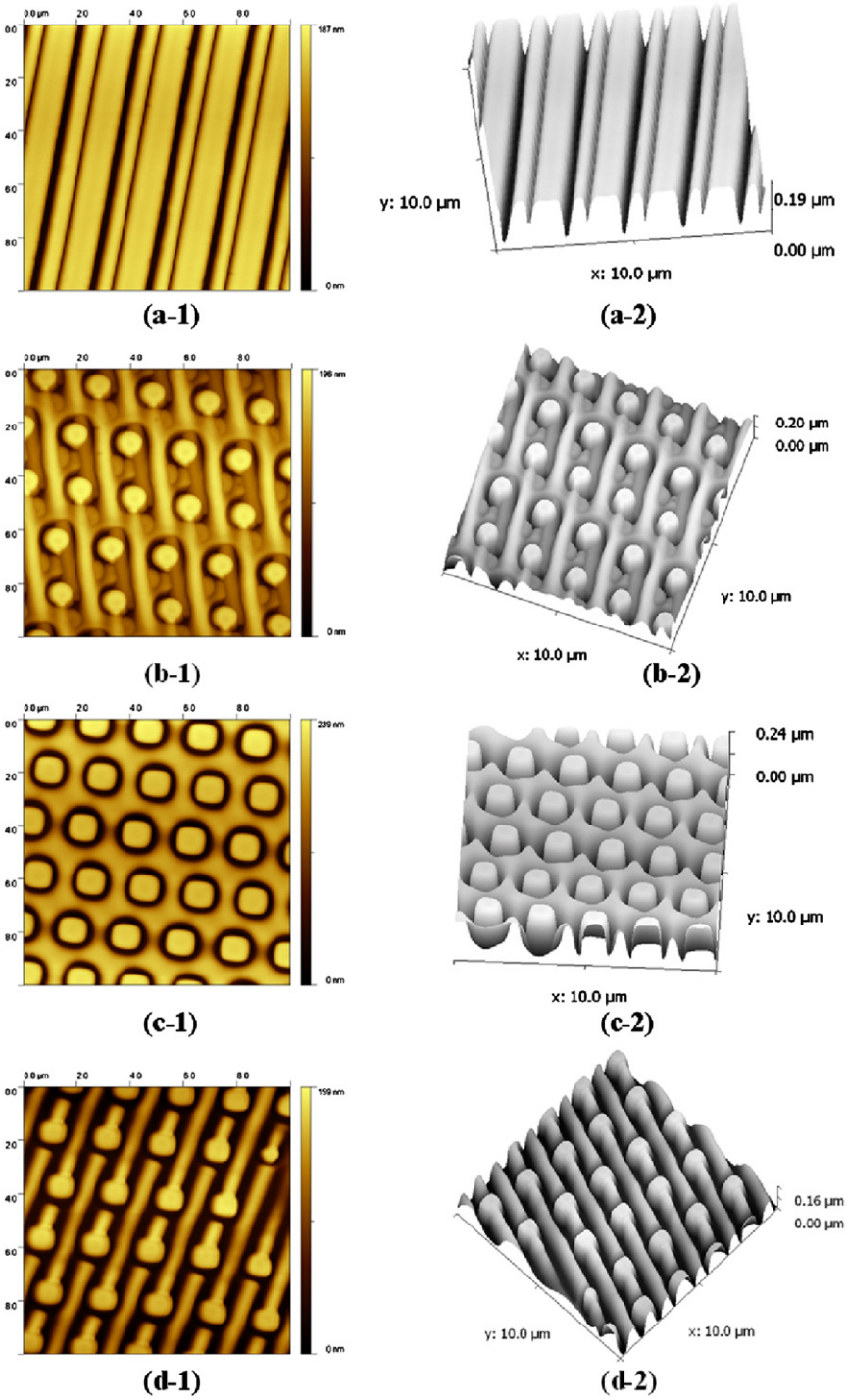


**Figure 6.** AFM images of 3D PDMS nanostructures in top (left) and 3D (right) views. (*a*-1, *a*-2) Asymmetric nanolines; (*b*-1, *b*-2) asymmetric nanocircles; (*c*-1, *c*-2) symmetric nanosquares; (*d*-1, *d*-2) asymmetric nanosquares.

100 $\mu$m $\times$ 100 $\mu$m to 500 $\mu$m $\times$ 500 $\mu$m for both nanocircles and nanosquares). Also, the resulting nanopatterns (both symmetric and asymmetric) are smooth with little profile variation (<5 nm) in the *x*–*y* directions. Uniformity of very large pattern areas such as over the extent of a 4 inch wafer and little edge roughness variation in resulting nanopatterns should be possible by ensuring uniform application of a sufficient and suitable force or pressure over the overall pattern area without deforming the PDMS stamp, requiring a properly designed INIL setup.

### *3.2. 3D Si nanostructures*

Figures 4 and 5 show representative SEM and AFM images of resulting 3D Si nanostructures produced by RIE pattern transfer. The width of the resulting Si symmetric nanolines

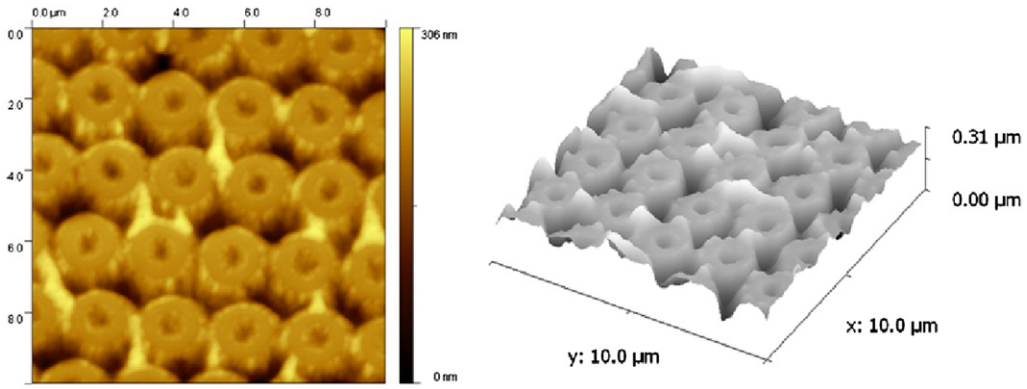


(*a*) (*b*)

**Figure 7.** AFM images of the PDMS stamp embedded with Si nanocircles in (*a*) top and (*b*) 3D views.

(figure 4(*a*)) is approximately 250 nm, equal to that of the original polymer nanolines (figure 3(*a*)), while their height is 200 nm, which is tunable by adjusting the process etching time. The resulting Si asymmetric nanolines (figures 4(*b*) and 5(*a*-1, *a*-2)) have similar morphology and dimensions to the original polymer asymmetric nanolines (figure 3(*b*)). This indicates that conformal 3D nanopattern transfer from the polymer resist mask to the Si substrate using plasma ($CHF_3/H_2$) dry etching has occurred. Similarly, 3D pattern transfer of Si symmetric and asymmetric nanocircles and nanosquares is also observed. The corners of the resulting Si nanosquares are slightly rounded (figures 4(*e*), (*f*), 5(*d*-1, *d*-2), and (*e*-1, *e*-2)), but are exact replicas of their polymer masks (figures 3(*e*) and (*f*)). These resulting 3D periodic Si nanostructures with multiple heights have great potential in a number of technological areas including application as angle-resolved photonic crystals that exploit and tune their optical properties owing to their structural characteristics.

### *3.3. 3D PDMS silicone nanostructures*

Figure 6 shows AFM images of the resulting PDMS silicone nanostructures. Careful comparisons indicate that the 3D nanostructures of Si mold masters are successfully transferred into the PDMS stamps. In fact, in order to successfully achieve 3D silicone nanostructures as designed an efficient de-molding operation is very important and challenging because of the significant surface adhesion and friction forces associated with nanotribology. In this work, this problem has been addressed by treating the Si mold template surface by an anti-adhesion agent (3,3,3-trifluoropropyl dimethylchlorosilane) prior to casting and curing PDMS prepolymer onto the Si mold template. Such an anti-adhesion agent can efficiently react with the template surface and form a thin layer homogenously covering the entire template surface. Such a thin layer is able to greatly reduce the adhesion and frictions between the Si template and cured PDMS during de-molding, ultimately leading to successful separation. In comparison, some samples without surface modification by this anti-adhesion agent were examined. For such systems, it was very hard to separate the cured PDMS stamp from the Si mold template. Applying brute force may separate them but can easily damage the Si template. Moreover, some of the broken Si nanostructure pieces can be easily embedded into the resulting PDMS stamp. Figure 7 shows AFM images typically observed in the PDMS stamp embedded with Si nanocircles resulting from an improper de-molding process. Such observations were actually also noticed and reported by Fujita *et al* [20] where they extensively studied such phenomena and further applied it for fabricating $PDMS/SiO_2$ nanocomposites with embedded uniform and regular $SiO_2$ nanostructures. Potential applications of these 3D silicone nanostructures include biomimicking of functional anisotropic surfaces and plastic fluidic devices.

### *3.4. 3D Au nanostructures*

Figures 8 and 9 show SEM and AFM images of resulting 3D Au nanostructures freestanding on adhesive polymer substrates. It is clearly seen from these images that the 3D nanopatterned Au thin films are correctly transferred from the PDMS stamps to the adhesive polymer substrates (e.g. Kapton tape and PU sheet) with very few cracks observed. The transferred metal thin film is Au (40 nm) with a 5 nm Ti film underneath functioning as an adhesion layer to the polymer substrate. The strong cohesion of Au [16] leads the entire Au thin film to be effectively transferred to an adhesive polymer substrate. A careful comparison of the resulting Au nanostructures with Si mold templates indicates that the nanostructures of varying heights are properly preserved in the freestanding Au thin film. However, complete elimination of nanocracks generated in the resulting Au 3D nanostructures is very challenging. These cracks are primarily attributed to the elastomeric stamp deformation during the operation of transfer printing, and Rogers *et al* have undertaken extensive studies on minimizing cracks in nTP by improving the stamp surface chemistries, thin film deposition techniques and stamp pattern design [21]. In our work, crack elimination has been effectively achieved by a combination of using a glass backing to support the PDMS stamp, coupled with a thin nanopatterned PDMS

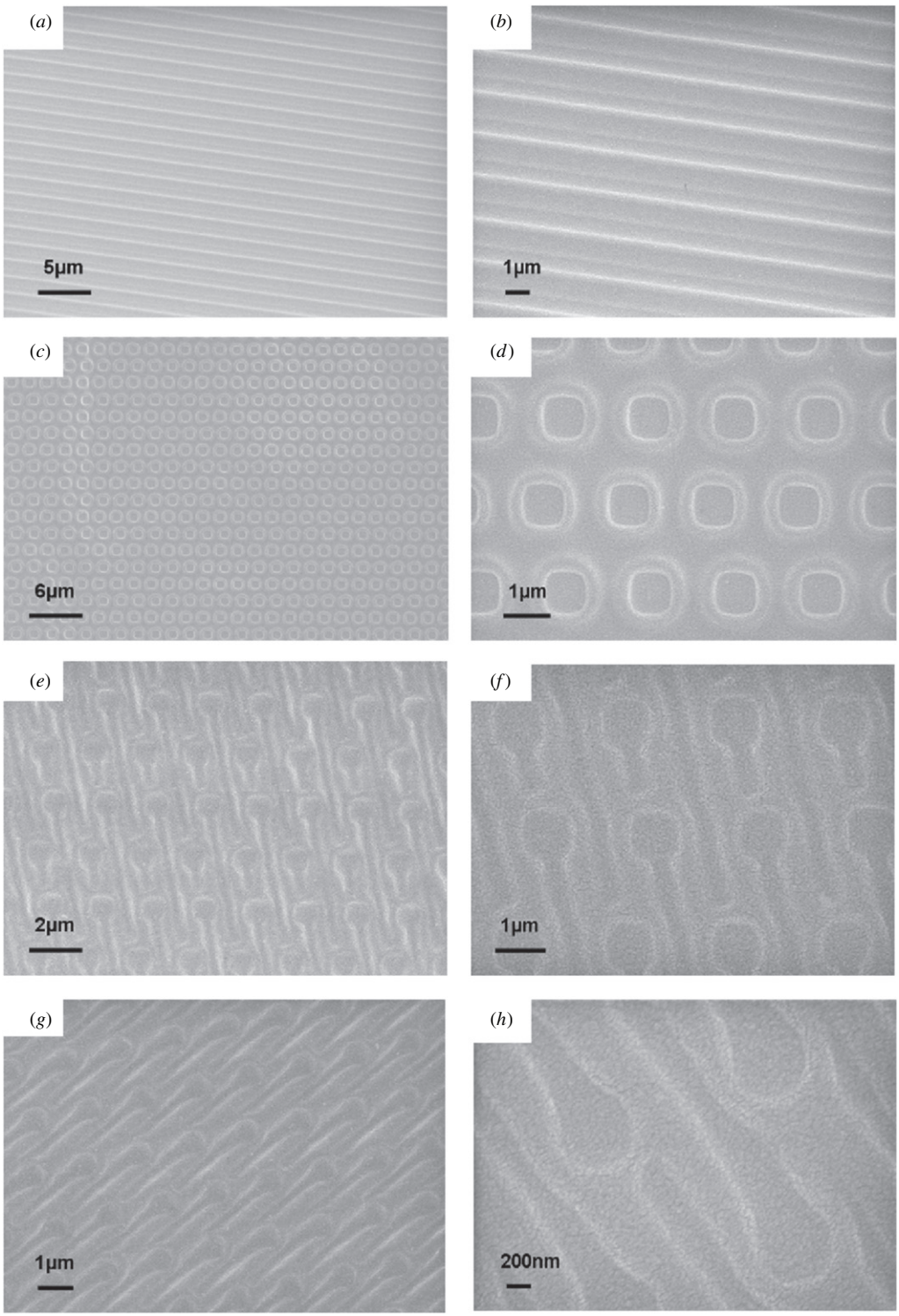


**Figure 8.** SEM images of 3D Au nanostructures freestanding on an adhesive glass substrate. (*a*), (*b*) Asymmetric nanolines; (*c*), (*d*) symmetric nanosquares; (*e*), (*f*) asymmetric nanosquares; (*g*), (*h*) asymmetric nanocircles.

stamp (approximately 0.5 mm thick), in addition to a gentle force. The demonstrated 3D Au nanostructures with multiple heights could be potentially utilized as plasmonic crystals that produce incident angle-dependent optical properties due to their asymmetric nanostructures, and consequently have wide applicability for sensing and imaging applications. Further, 3D anisotropic or chiral nanostructures could be potentially assembled layer-by-layer from the demonstrated nanopatterned Au film with multiple feature heights. Such stacked 3D anisotropic structures would be of great interest since they may bring interesting and novel properties ranging from condensed matter physics to optics for various potential

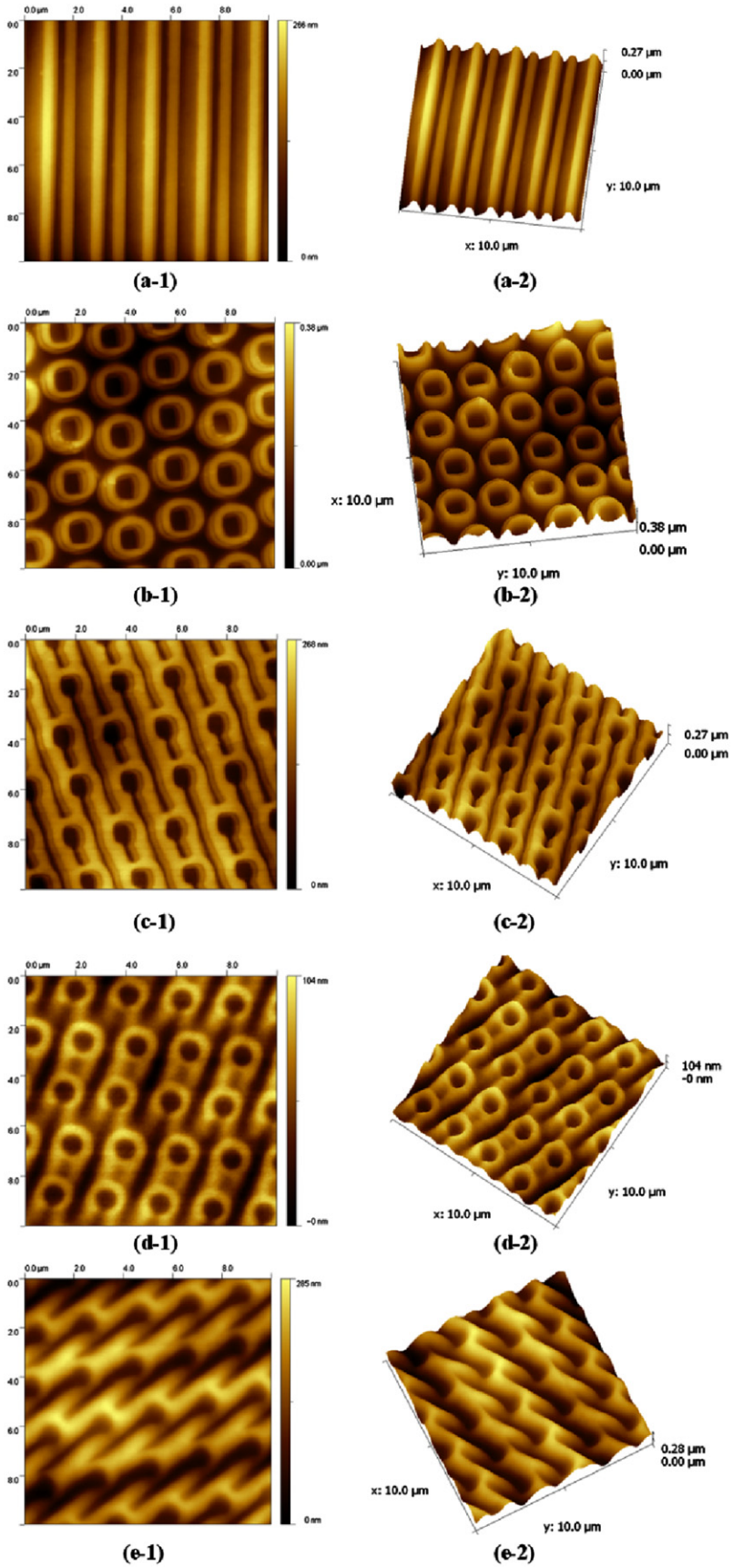


**Figure 9.** AFM images of 3D Au nanostructures in top (left) and 3D views (right). (*a*-1, *a*-2) Asymmetric nanolines; (*b*-1, *b*-2) and (*c*-1, *c*-2) symmetric and asymmetric nanosquares; (*d*-1, *d*-2) and (*e*-1, *e*-2) asymmetric nanocircles with different degrees of asymmetry.

applications. The INIL-based process demonstrated in this work could serve as a significant technical driver for such exploration.

## 4. Conclusion

In this paper, an integrated 'top–down' 3D nanofabrication strategy has been demonstrated by combining inclined nanoimprinting lithography (INIL) with reactive ion etching (RIE), micro-contact molding and metal nanotransfer printing (nTP). It enables the pattern transfer of various 3D nanostructures with varying heights from a polymer resist layer to other material media including an Si-based substrate, a PDMS silicone stamp and a metal Au thin film in a controlled way, with reduced fabrication cost and complexity. Various 3D nanostructures can be designed, produced and properly preserved in a variety of target materials by using such an integrated process. Applications of these 3D nanostructures could be angle-resolved photonic crystals, plasmonic crystals and bio-mimicking anisotropic self-cleaning surfaces. Therefore, the reported INIL-based 3D nanofabrication shows great application potential in photonics, plasmonics, nanotribology and NEMS.

## References


[1] Ishizaki K and Noda S 2009 *Nature* **460** 367–70
[2] Freymann G, Ledermann A, Thiel M, Staude I, Essig S, Busch K and Wegener M 2010 *Adv. Funct. Mater.* **20** 1038–52
[3] Toader O and John S 2001 *Science* **292** 1133–5
[4] Qi M, Lidorikis E, Rakich P, Johnson S, Joannopoulos J, Ippen E and Smith H 2004 *Nature* **429** 538–42
[5] Subramania G, Lee Y-J, Brener I, Luk T S and Clem P G 2007 *Opt. Express* **15** 12049–57
[6] Sun Q, Juodkazis S, Murazawa N, Mizeikis V and Misawa H 2010 *J. Micromech. Microeng.* **20** 035004
[7] Jeon S *et al* 2007 *Opt. Express* **15** 6358–66
[8] Baumberg J, Kelf T, Sugawara Y, Cintra S, Abdelsalam M, Bartlett P and Russell A 2005 *Nano Lett.* **5** 2262–7
[9] Baca A, Truong T, Cambrea L, Montgomery J, Gray S, Abdula D, Banks T, Yao J, Nuzzo R and Rogers J 2009 *Appl. Phys. Lett.* **94** 243109
[10] Heo C, Kim S, Jang S, Lee S and Yang S 2009 *Adv. Mater.* **21** 1726–31
[11] Stewart M, Mack N, Malyarchuk V, Soares J, Lee T, Gray S, Nuzzo R and Rogers J 2006 *Proc. Natl Acad. Sci.* **103** 17143–8
[12] Kinkhabwala A, Yu Z, Fan S, Avlasevich Y, Mullen K and Moerner W 2009 *Nature Photonics* **3** 654–7
[13] Prodan E, Radloff C, Halas N and Nordlander P 2003 *Science* **302** 419–22
[14] Kan T, Matsumoto K and Shimoyama I 2010 *J. Micromech. Microeng.* **20** 085032
[15] Liu Z, Bucknall D G and Allen M G 2007 *Proc. Transducers 2007 & Eurosensors XXI Dig. Techn. Papers* **1–2** U819–20
[16] Zaumseil J, Meitl M, Hsu J, Acharya B, Baldwin K, Loo Y and Rogers J 2003 *Nano Lett.* **3** 1223–7
[17] Medeiros D R, Aviram A, Guarnieri C R, Huang W S, Kwong R, Magg C K, Mahorowala A P, Moreau W M, Petrillo K E and Angelopoulos M 2001 *IBM J. Res. Dev.* **45** 639–50
[18] Hui C Y, Jagota A, Lin Y Y and Kramer E J 2002 *Langmuir* **18** 1394–407
[19] Odom T W, Love J C, Wolfe D B, Paul K E and Whitesides G 2002 *Langmuir* **18** 5314–20
[20] Jalabert L, Bottier C, Kumemura M and Fujita H 2009 *J. Vac. Sci. Technol.* B **27** 3055–8
[21] Menard E, Bilhaut L, Zaumseil J and Rogers J 2004 *Langmuir* **20** 6871–8
[22] Liu Z, Bucknall D G and Allen M G 2011 *Nanotechnology* **22** 225302